IEEE Access
Multidisciplinary ⋮ Rapid Review ⋮ Open Access Journal

Received December 9, 2020, accepted December 14, 2020, date of publication December 18, 2020,
date of current version December 31, 2020.

*Digital Object Identifier 10.1109/ACCESS.2020.3045587*

# Improvement of Concentration Inversion Model Based on Second Harmonic Valley Spacing in Wavelength Modulation Spectroscopy

**YUN PAN[1,2], YI LI[1], CHANGXIANG YAN[1,3], JING YUAN[1,2], AND YIJIE REN[1,2]**
[1]Changchun Institute of Optics, Fine Mechanics and Physics, Chinese Academy of Sciences, Changchun 130033, China
[2]College of Materials Science and OptoElectronic Technology, University of Chinese Academy of Sciences, Beijing 100049, China
[3]Center of Materials Science and Optoelectrics Engineering, University of Chinese Academy of Science, Beijing 100049, China

Corresponding author: Changxiang Yan (yancx@ciomp.ac.cn)

This work was supported in part by the National Key Research and Development Program of China under Grant 2016YFF0103603; in part by the Technology Development Program of Jilin Province, China, under Grant 20180201012GX; in part by the National Natural Science Foundation of China (NSFC) under Grant 61627819, Grant 61727818, Grant 6187030909, and Grant 61875192; in part by the National Natural Science Foundation of China Youth Fund under Grant 61805235; and in part by STS Project of Chinese Academy of Sciences under Grant KFJ-STS-SCYD-212, Grant KFJ-STS-ZDTP-049, and Grant KFJ-STS-ZDTP-057.

**ABSTRACT** In tunable diode laser absorption spectroscopy (TDLAS), the wavelength modulation spectroscopy (WMS) is widely employed. However, when measuring the gas concentration with the second harmonic signal, errors will occur and the inversion accuracy will be reduced, because the change of the modulation depth will lead to the change of the second harmonic peak value, and the value of modulation depth cannot be calculated directly in the absence of gas component. To improve the inversion accuracy of WMS technology, we calibrate the modulation depth and take it as a parameter to the concentration inversion model. In this article, the relationship between the modulation depth and the valley spacing of the second harmonic is first derived, and used to calibrate the modulation depth in the measurement; then, an improved concentration inversion model is established by adding the calibrated modulation depth to the traditional model. Through simulations in Simulink and gas concentration measurement experiments with carbon monoxide (CO), the effectiveness of modulation depth calibration using valley spacing and the accuracy of the improved model are verified. The gas concentration measurement error of the improved model (relative error $< 0.37\%$, root-mean-square error (RMSE): $5.468 \times 10^{-5}$) is reduced by nearly one order of magnitude compared to the traditional model without calibration of the modulation depth (relative error $< 1.70\%$, RMSE: $2.178 \times 10^{-4}$). The correction method of modulation depth in this article does not need the priori information of the gas component, and the improved model produces a better determination of gas concentration immune to the variations of modulation depth, which is important for field measurements especially those with large environmental variations.

**INDEX TERMS** Concentration inversion model, modulation depth, TDLAS, valley spacing, WMS.

## I. INTRODUCTION

In thermal power plants, in-situ real-time monitoring of carbon monoxide (CO) concentration is of great significance for energy saving and emission reduction. The tunable diode laser absorption spectroscopy (TDLAS) technology [1] is a technology that utilizes the tunable diode laser to scan the absorption line of the gas, thereby measuring various parameters such as concentration, temperature [7], flow velocity [8], and so on. In recent years, with the development and maturity of optoelectronic devices [2]–[6], this technology has been widely employed in atmospheric environment monitoring [9], industrial process control [10], combustion flow field diagnosis [11], and human breath detections [12], due to its advantages of high sensitivity, high selectivity, fast response speed, and in-situ real-time measurement. TDLAS technology mainly contains two measurement methods, namely the direct absorption spectroscopy (DAS) technology [13] and wavelength modulation spectroscopy (WMS) technology [14]. Compared with DAS, WMS technology can effectively reduce the influence of noise on the detection signal and achieve higher detection accuracy, and is more widely used.

In WMS, the laser wavelength is simultaneously affected by a low frequency scanning signal and a high frequency

The associate editor coordinating the review of this manuscript and approving it for publication was Qingli Li.

modulation signal. After the laser being absorbed by the gas, a lock-in amplifier (LIA) is used to detect the harmonic signal of the transmitted laser intensity. The concentration is inversed using the peak value of the second harmonic ($2f$) signal. In actual applications, the environmental parameters and modulation parameters of the modulation signal have an important influence on the $2f$ lineshape. Among these parameters, the modulation depth is related to both environmental and modulation parameters, which will bring errors to the concentration inversion results and limit the applications of WMS technique.

Researches have studied the influence of modulation depth on $2f$ signals. Kluczynski and Axner *et al.* [15]–[18] gave the non-complex analytical expression for the $n$th Fourier component of the Lorentzian lineshape, which is the function of modulation depth. Some researches selected the proper modulation parameters to optimize the $2f$ signal through simulations and experiments [19]–[23]. Parameters such as mechanical vibration, etalon effect, temperature, and pressure will affect the real modulation index. Chang *et al.* and Guo *et al.* eliminated these influences using toroidal absorption cell and calibration-free modulation spectroscopy [24], [25]. Chen *et al.* [26] determined the modulation amplitude from the distance between the zero crossings of the $2f$ signal, and utilized this relationship to characterize the frequency modulation response of the diode laser. Some researchers studied the relationship between the modulation depth and temperature and pressure, and obtained the empirical formula for temperature and pressure correction [27].

However, the modulation depth cannot be calculated directly from the measured temperature and pressure when the gas component is unknown. Besides, in those researches, the modulation depth was either taken as a constant in the measurement, or not fully corrected in terms of modulation amplitude and temperature and pressure.

Aiming at this problem, we first derived the simplified relationship between the modulation depth and the valley spacing of the $2f$ signal, and used this relationship to calibrate the modulation depth in the measurement; Then an improved concentration inversion model was established using the simplified relationship between the modulation depth and the peak value of the $2f$ signal, where the modulation depth calibrated above was taken as a parameter.

The rest of this article is organized as follows: Section II is the description of the fundamentals of WMS, the calibration method of the modulation depth, and the improved concentration inversion model. The results of the simulations are in Section III. Section IV is the experimental setup. The experimental results and discussions are in Section V. Section VI presents the conclusions of this article.

## II. THEORY ANALYSIS

In this section, we present the theoretical description of our model. On one hand, the modulation depth was calibrated using the relationship with the valley spacing of the $2f$ signal; On the other hand, we further proposed an improved concentration inversion model with the calibrated modulation depth as a parameter.

### A. FUNDAMENTALS OF WMS

In WMS technology, the laser output frequency-time response after injecting a high-frequency sinusoidal modulation signal is expressed as in (1) [28]:

$$\nu = \bar{\nu} + a\cos(\omega t) \tag{1}$$

where $\bar{\nu}$ (in $\mathrm{cm}^{-1}$) is the average frequency of the laser driven by the sawtooth wave scanning signal, and the scanning range is $\Delta\nu$ (in $\mathrm{cm}^{-1}$), $a$ (in $\mathrm{cm}^{-1}$) is the frequency modulation (FM) amplitude and $\omega$ is the angular frequency of the modulation signal.

Considering the nonlinear intensity modulation (IM) and the phase shift between IM and FM of the laser, the output instantaneous laser intensity can be expressed as the combination of the linear and nonlinear parts [29]:

$$I_0(t) = \overline{I_0} + \Delta I_1\cos(\omega t + \psi_1) + \Delta I_2\cos(2\omega t + \psi_2) \tag{2}$$

where $\bar{I}_0$ (in mW) is the average laser intensity driven by the scanning signal, $\Delta I_1$ and $\Delta I_2$ are the amplitude of linear and nonlinear laser IM respectively, their values are related to the FM amplitude; $\psi_1$ and $\psi_2$ are the phase shift between linear and nonlinear IM and FM respectively, $\psi_2$ is also related to the FM amplitude.

When the laser passes through the gas, the transmitted laser intensity and the initial laser intensity follow the Lambert-Beer law [21], and the transmittance coefficient is as follows:

$$\begin{aligned}\tau(\nu) &= \left(\frac{I_t(t)}{I_0(t)}\right)_\nu \\ &= \exp[-\alpha(\nu)] \\ &\approx 1-\alpha(\nu) \\ &= 1 - PS(T)\,\phi(\nu)\,CL\end{aligned} \tag{3}$$

where $P$ (in atm) is the total pressure of the mixed gas, $S(T)$ (in $\mathrm{cm}^{-2}\cdot\mathrm{atm}^{-1}$) is the line strength of the gas absorption feature at the temperature $T$ (in K), $\phi(\nu)$ (in cm) is the lineshape function of the gas absorption feature, $C$ (in volume fraction) is the concentration of the gas to be measured, $L$ (in cm) is the effective optical path length, and $\alpha(\nu)$ is the spectral absorbance and can be expanded into the form of Fourier cosine series [21]:

$$-\alpha[\bar{\nu} + a\cos(\omega t)] = \sum_{n=0}^{\infty} H_n(\bar{\nu}, a)\cos(n\omega t) \tag{4}$$

where $H_n$ is the $n$th order Fourier coefficient of absorption, given by:

$$\begin{cases} H_0(\bar{\nu}, a) = -\dfrac{1}{2\pi}\displaystyle\int_{-\pi}^{\pi}\alpha[\bar{\nu} + a\cos(\theta)]d\theta \\ \qquad\qquad = -\dfrac{PS(T)CL}{2\pi}\displaystyle\int_{-\pi}^{\pi}\phi[\bar{\nu} + a\cos(\theta)]d\theta \\ H_n(\bar{\nu}, a) = -\dfrac{1}{\pi}\displaystyle\int_{-\pi}^{\pi}\alpha[\bar{\nu} + a\cos(\theta)]\cos(n\theta)\,d\theta \\ \qquad\qquad = -\dfrac{PS(T)CL}{\pi}\displaystyle\int_{-\pi}^{\pi}\phi[\bar{\nu} + a\cos(\theta)]\cos(n\theta)\,d\theta \end{cases} \tag{5}$$

The gas absorption lineshape function is described by the Lorentzian lineshape [30], [31]:

$$\phi(\nu) = \frac{1}{2\pi} \frac{\Delta\nu_c}{(\nu - \nu_0)^2 + \left(\Delta\nu_c/2\right)^2} \tag{6}$$

where $\nu_0$ (in $\mathrm{cm}^{-1}$) is the central frequency and $\Delta\nu_c$ (in $\mathrm{cm}^{-1}$) is the full width at half maximum (FWHM) of the gas absorption feature. The Lorentzian full width of the line can be expressed as follows:

$$\Delta\nu_c = 2P \sum_j \left(\frac{T_0}{T}\right)^{n_j} \gamma_j(T_0, P_0) X_j \tag{7}$$

where $X_j$ is the mole fraction of component j, $\gamma_j$ (in $\mathrm{cm}^{-1}$/atm) is the Lorentzian half width at half maximum (HWHM) coefficient for broadening by component j at $T_0 = 296$ K and $P_0 = 1$ atm, $n_j$ is the temperature-dependence exponent for $\gamma_j$ [32].

Define two parameters:

$$x = \frac{\bar{\nu} - \nu_0}{\Delta\nu_c/2} \tag{8}$$

$$m = \frac{a}{\Delta\nu_c/2} \tag{9}$$

where $x$ is the normalized center frequency detuning and $m$ is the modulation depth. Then (5) can be rewritten as follows:

$$\begin{cases} H_0(x, m) = -\dfrac{PS(T)CL}{\pi \cdot \Delta\nu_c/2} \displaystyle\int_{-\pi}^{\pi} \frac{1}{2\pi} \cdot \frac{1}{(x + m\cos\theta)^2 + 1} d\theta \\ H_n(x, m) = -\dfrac{PS(T)CL}{\pi \cdot \Delta\nu_c/2} \displaystyle\int_{-\pi}^{\pi} \frac{1}{\pi} \cdot \frac{\cos(n\theta)}{(x + m\cos\theta)^2 + 1} d\theta \end{cases} \tag{10}$$

It can be seen from (10) that, $H_n$ is a function of $x$, $m$ and $C$. The expression of transmitted laser intensity can be written as follows by combining (2), (3) and (4):

$$\begin{aligned} I_t(t) &= I_0(t) \exp[-\alpha(\nu)] \\ &\approx I_0(t)[1 - \alpha(\nu)] \\ &= \left[1 + \sum_{n=0}^{\infty} H_n(x, m) \cos(n\omega t)\right] \\ &\times \left[\overline{I_0} + \Delta I_1 \cos(\omega t + \psi_1) + \Delta I_2 \cos(2\omega t + \psi_2)\right] \end{aligned} \tag{11}$$

The $2\omega$-frequency component in the transmitted laser intensity is as follows:

$$\begin{aligned} I_{2f}(t) &= \overline{I_0} H_2 \cos(2\omega t) \\ &+ \frac{1}{2}\Delta I_1 [H_1 \cos(2\omega t + \psi_1) + H_3 \cos(2\omega t - \psi_1)] \\ &+ \Delta I_2 \left[(1 + H_0)\cos(2\omega t + \psi_2) + \frac{1}{2} H_4 \cos(2\omega t - \psi_2)\right] \end{aligned} \tag{12}$$

The reference signal of the LIA used to extract the $2\omega$-frequency component is as follows:

$$I_{ref} = \cos(2\omega t) \tag{13}$$

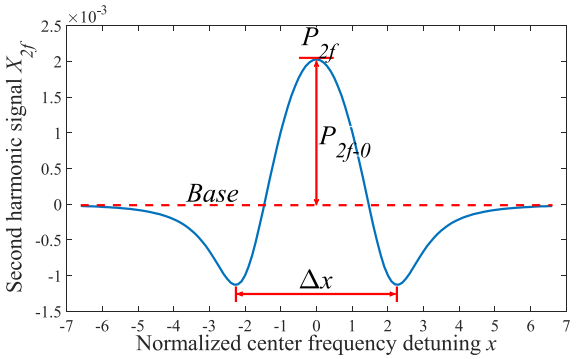


**FIGURE 1.** Schematic diagram for second harmonic signal.

After the LIA and low-pass filter, the high-frequency signals are filtered out, the extracted $2f$ signal is shown in (14), and the waveform is shown in Fig. 1.

$$\begin{aligned} X_{2f} &= \frac{1}{2}\overline{I_0} H_2 + \frac{1}{4}\Delta I_1 (H_1 + H_3)\cos(\psi_1) \\ &+ \frac{1}{2}\Delta I_2 \left(1 + H_0 + \frac{1}{2} H_4\right)\cos(\psi_2) \end{aligned} \tag{14}$$

From Eq. (10), it can be known that when there is no gas absorption, $C = 0$, and $H_n = 0$, then the $2f$ signal is the baseline, and (14) can be written as:

$$Base = X_{2f,0} = \frac{1}{2}\Delta I_2 \cos(\psi_2) \tag{15}$$

Combining (14) and (15), we can obtain the expression of the $2f$ signal after subtracting the baseline as follows:

$$\begin{aligned} X_{2f-0} &= X_{2f} - X_{2f,0} \\ &= \frac{1}{2}\overline{I_0} H_2(x, m) + \frac{1}{4}\Delta I_1 [H_1(x, m) + H_3(x, m)]\cos(\psi_1) \\ &+ \frac{1}{2}\Delta I_2 \left[H_0(x, m) + \frac{1}{2} H_4(x, m)\right]\cos(\psi_2) \end{aligned} \tag{16}$$

When $x = 0$, $X_{2f-0}$ reaches the maximum value $P_{2f-0}$, which is the peak value of the $2f$ signal. The expression is given by:

$$P_{2f-0} = \frac{1}{2}\overline{I_0} H_2(0, m) + \frac{1}{2}\Delta I_2 \left[H_0(0, m) + \frac{1}{2} H_4(0, m)\right]\cos(\psi_2) \tag{17}$$

From Eq. (17), it can be seen that $P_{2f-0}$ is a function of $m$. Research shows that when m is 2.2, $P_{2f-0}$ reaches the maximum [15]. Since $H_n$ is proportional to $C$, $P_{2f-0}$ is also proportional to $C$. The traditional concentration inversion uses the linear relationship between the peak value of $2f$ signal and the concentration, and the expression is given by:

$$C = \frac{P_{2f-0}}{k} \tag{18}$$

where $k$ is the coefficient of the inversion model and is often taken as a constant after setting modulation depth $m$ to the optimum value. However, the changes of $m$ in measurement will cause the changes in $k$, thereby bring errors to concentration inversion.

### B. CALIBRATION OF MODULATION DEPTH

According to the analysis in Section A, to eliminate the error caused by the change of modulation depth $m$, it is necessary to correct the value of $k$, so it is necessary to know the real value of modulation depth. As we can see in (7) and (9), the Lorentzian full width $\Delta\nu_c$ and modulation depth $m$ is related to the temperature, pressure, mole fraction, Lorentzian HWHM coefficient and temperature-dependent exponent of the gas component. The temperature and pressure can be measured, but the gas component is unknown in real applications, thus the modulation depth cannot be calibrated directly.

According to Fig. 1 and (16), there is a minimum value $V_{2f-0}$ for the baseline-subtracted $2f$ signal $X_{2f-0}$, the expression is as follows:

$$\begin{aligned} V_{2f-0} &= X_{2f-0}(x_1) \\ &= \frac{1}{2}\overline{I_0}H_2(x_1,m) + \frac{1}{4}\Delta I_1\left[H_1(x_1,m)\right. \\ &\quad \left.+H_3(x_1,m)\right]\cos(\psi_1) \\ &\quad +\frac{1}{2}\Delta I_2\left[H_0(x_1,m)+\frac{1}{2}H_4(x_1,m)\right]\cos(\psi_2) \end{aligned} \tag{19}$$

where $x_1$ is the abscissa when $X_{2f-0}$ taking the minimum value.

Since the second harmonic curve has two minimum values on both sides, the abscissa of the other minimum value is denoted as $x_2$. Therefore, as seen in Fig. 1, we define the horizontal distance between the two minimum values of the $2f$ signal as the valley spacing, which is marked as $\Delta x$. The expression is given by:

$$\Delta x = |x_1 - x_2| \tag{20}$$

For different values of $m$, $x_1$, $x_2$ and $\Delta x$ are also different. By setting different values of $m$ and other parameters, we can obtain the corresponding $x_1$, $x_2$ and $\Delta x$ values. Setting $m$ to the value of 2.2 and several nearby values, we obtained the scatter plot of $\Delta x$ versus $m$ as follows:

From the above figure, it can be seen that $\Delta x$ and $m$ can be fitted into a linear relationship, and the expression is as follows:

$$\Delta x = a_1 \times m + a_2 \tag{21}$$

where $a_1$ and $a_2$ are different according to the actual measurement condition and need to be calibrated in advance during the measurement.

By extracting the valley spacing of the $2f$ signal, we can calculate the value of $m$ according to (21), the expression of $m$ is as follows:

$$m = b_1 \times \Delta x + b_2 \tag{22}$$

### C. IMPROVED CONCENTRATION INVERSION MODEL

After calibrating the modulation depth, we can correct the value of $k$ in (18).

Define a parameter $S_n(x, m)$, given by:

$$S_n(x,m) = H_n(x,m)\big/C \tag{23}$$

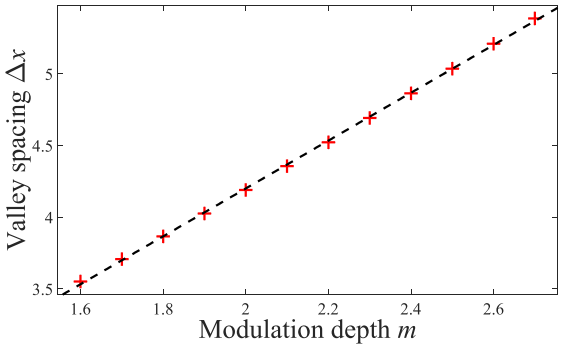


**FIGURE 2.** Theoretical scatter plot of valley spacing $\Delta x$ versus modulation depth $m$.

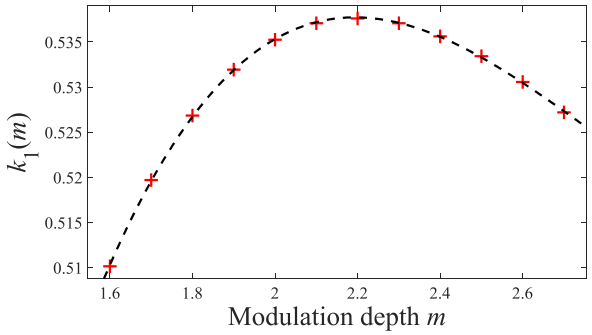


**FIGURE 3.** Theoretical scatter plot of $k_1(m)$ versus modulation depth $m$.

It can be known from (10) that:

$$\begin{cases} S_0(x,m) = -\dfrac{PS(T)L}{\pi\Delta\nu_c/2}\cdot\displaystyle\int_{-\pi}^{\pi}\frac{1}{2\pi}\cdot\frac{1}{(x+m\cos\theta)^2+1}\,d\theta \\ S_n(x,m) = -\dfrac{PS(T)L}{\pi\Delta\nu_c/2}\cdot\displaystyle\int_{-\pi}^{\pi}\frac{1}{\pi}\cdot\frac{\cos(n\theta)}{(x+m\cos\theta)^2+1}\,d\theta \end{cases} \tag{24}$$

Then the concentration inversion model can be written as follows:

$$C = \frac{P_{2f-0}}{\frac{1}{2}\overline{I_0}S_2(0,m) + \frac{1}{2}\Delta I_2\left[S_0(0,m)+\frac{1}{2}S_4(0,m)\right]\cos(\psi_2)} \tag{25}$$

Compared with (18), $k$ is replaced by the function of $S_n$ in (25). It can be seen from (24) that the expression of $S_n$ is relatively complicated, if it is directly used in (25), the concentration calculation will be quite difficult. Therefore, an apposite function $k_1(m)$ is chosen to simplify the denominator in (25). Using the same values of $m$ as in Section B, we obtained the scatter plot of $k_1(m)$ versus $m$, as shown in Fig. 3.

By comparing the fitting results of the 1st to 5th degree polynomials, we find that when choosing the 3rd degree polynomial, the fitting accuracy is far higher than the concentration measurement accuracy, the expression is shown in (26):

$$k_1(m) = c_1 \times m^3 + c_2 \times m^2 + c_3 \times m + c_4 \tag{26}$$

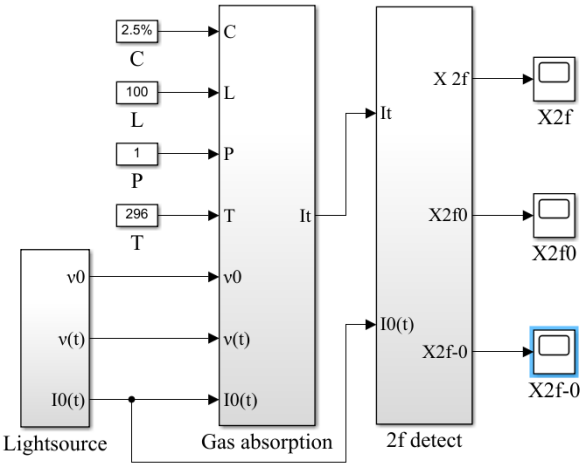


**FIGURE 4.** Schematic diagram for the overall simulation system.

where $c_1$, $c_2$, $c_3$, and $c_4$ are also different in different conditions.

After obtaining the simplified expression of $k_1(m)$, we can establish the concentration inversion model as follows:

$$C = \frac{P_{2f-0}}{c_1 \times m^3 + c_2 \times m^2 + c_3 \times m + c_4} \tag{27}$$

where $m$ is obtained from (22).

## III. SIMULATIONS

### A. SIMULATION SYSTEM

The simulation system is established using the Simulink module in Matlab. The frequency of the sawtooth wave scanning signal of the simulation system is 5 Hz, the frequency of the sine wave modulation signal is 2000 Hz, the frequency of the nonlinear laser IM and the reference signal is 4000 Hz, the sampling frequency is 200 kHz, the simulation start time is 0s, and the end time is 0.2s. The schematic diagram of the overall simulation system is shown in Fig. 4. The parameters are set as follows: $\nu_0 = 6383.09\ \text{cm}^{-1}$, $\Delta\nu = \pm 0.45\ \text{cm}^{-1}$, $\bar{I}_0 = 13.26$ mW, $L = 100$ cm, $P = 1$ atm, $T = 296$ K, according to the CO gas absorption parameters in HITRAN database [32], $S(T) = 5.011 \times 10^{-4}\ \text{cm}^{-2}\cdot\text{atm}^{-1}$, $\Delta\nu_c = 0.135\ cm^{-1}$.

### B. PARAMETER FITTING

In the above Simulink system, by changing the value of frequency modulation amplitude $a$ and concentration $C$, we can obtain the corresponding $2f$ signal, and calculate the value of modulation depth $m$, peak value $P_{2f-0}$, and valley spacing $\Delta x$ as the parameter fitting database, which is shown in Table 1.

Notice that in the simulations and real experiments, the abscissa of the $2f$ signal observed in the oscilloscope is time, the time difference between the two minimum values is recorded as $\Delta t$. The relationship between $\Delta x$ and $\Delta t$ is as follows:

$$\Delta x = \frac{\Delta t}{T_S} \cdot \frac{\Delta \nu}{\Delta \nu_c / 2} \tag{28}$$

where $T_S$ is the period of the sawtooth wave scanning signal. Here $T_S$ is 0.2 s.

**TABLE 1.** Parameter Fitting Dataset in Simulations.

| $C$ | $m$ | $P_{2f-0}$ | $\Delta x$ |
|---|---|---|---|
| 0.5% | 2.53 | 0.002098 | 5.108 |
| 1.0% | 1.98 | 0.004194 | 4.186 |
| 1.5% | 1.65 | 0.006054 | 3.665 |
| 2.0% | 2.31 | 0.008457 | 4.733 |
| 2.5% | 2.42 | 0.01054 | 4.920 |
| 3.0% | 1.87 | 0.01248 | 4.010 |
| 3.5% | 2.09 | 0.01475 | 4.367 |
| 4.0% | 2.20 | 0.01692 | 4.549 |
| 4.5% | 1.76 | 0.01843 | 3.837 |
| 5.0% | 2.64 | 0.02081 | 5.300 |

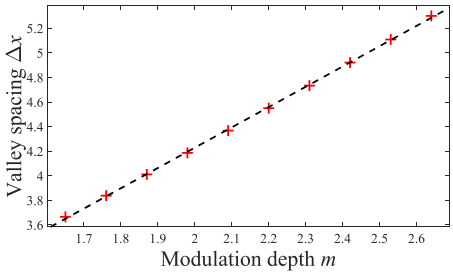


**FIGURE 5.** Scatter plot of valley spacing $\Delta x$ versus modulation depth $m$ in simulations.

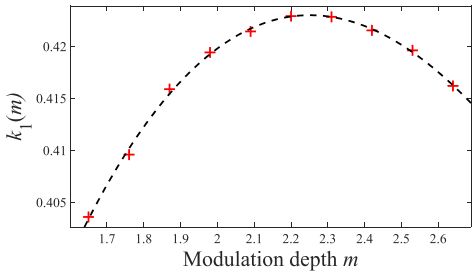


**FIGURE 6.** Scatter plot of $k_1(m)$ versus modulation depth $m$ in simulations.

The scatter plot of $\Delta x$ versus $m$ and the scatter plot of $k_1(m)$ versus $m$ using the parameter fitting dataset are shown in Fig. 5 and Fig. 6 respectively, which are consistent with the theoretical scatter plots in Fig. 2 and Fig. 3.

According to (22) and (27), we obtained the fitting results as shown in (29) and (30):

$$m = 0.605 \times \Delta x - 0.558 \tag{29}$$

$$C = \frac{P_{2f-0}}{9.783 \times 10^{-3} m^3 - 0.1144 m^2 + 0.3665 m + 0.06627} \tag{30}$$

The fitted RMSE of modulation depth $m$ is $5.563 \times 10^{-3}$, and $R^2$ is 99.97%. The fitted RMSE of concentration $C$ is $3.504 \times 10^{-5}$, and $R^2$ is 1.

For comparison, the traditional concentration inversion model as in (18) was also used for parameter fitting,

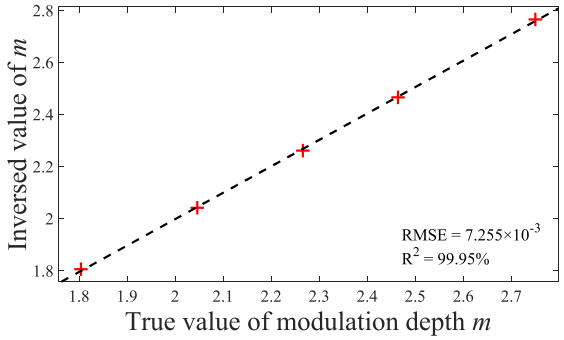


**FIGURE 7.** Scatter plot of inversed values versus true values of modulation depth $m$ in simulations.

**TABLE 2.** Validation Dataset and Results in Simulations.

| $C$ | $m$ | $P_{2f\text{-}0}$ | $\Delta x$ | $m_1$ | $C_1$ | $C_2$ |
|---|---|---|---|---|---|---|
| 1.2% | 2.266 | 0.005081 | 4.659 | 2.260 | 1.201% | 1.219% |
| 2.3% | 2.750 | 0.009506 | 5.492 | 2.764 | 2.308% | 2.280% |
| 3.2% | 1.804 | 0.01321 | 3.905 | 1.805 | 3.201% | 3.167% |
| 4.3% | 2.464 | 0.01808 | 4.996 | 2.465 | 4.294% | 4.336% |
| 5.5% | 2.046 | 0.02312 | 4.296 | 2.041 | 5.492% | 5.544% |

the expression is shown in (31). The fitted RMSE of concentration $C$ is $3.880 \times 10^{-4}$, and $R^2$ is 99.93%.

$$C = \frac{P_{2f-0}}{0.417} \tag{31}$$

### C. VALIDATION AND COMPARISON

According to (29) to (31), we calculated the values of $m$ and $C$ using the model validation dataset, and the results are shown in Table 2, where $m_1$ and $C_1$ are the inversed values using the improved model and $C_2$ is the values using traditional model.

The scatter plot of inversed values versus true values of $m$ is shown in Fig. 7, which indicates a high calibration accuracy of the modulation depth (RMSE $= 7.255 \times 10^{-3}$, $R^2 = 99.95\%$) and verifies the effectiveness of the calibration model using the valley spacing.

From Table 2, it can be calculated that the RMSE between $C_1$ and $C$ is $5.766 \times 10^{-5}$ and $R^2$ is 1, the RMSE between $C_2$ and $C$ is $3.179 \times 10^{-4}$ and $R^2$ is 99.96%. In addition, the absolute value of relative errors between the inversed value and true value of concentration were also calculated, the scatter plot is shown in Fig. 8.

It can be seen from Table 2 and Fig. 8 that compared to the traditional model (RMSE $= 3.179 \times 10^{-4}$), the RMSE of the improved model ($5.766 \times 10^{-5}$) is one order lower, and the absolute value of relative error of the improved model ($<0.35\%$) is nearly five times lower than that of the traditional model ($<1.54\%$).

## IV. EXPERIMENTAL SETUP

Figure 9 is the photo of experimental setup for gas concentration measurement with TDLAS, where the CO gas with a fixed volume fraction of 2.5% is used. The experimental system is powered by a three-channel DC power supply (GWInstek, GPP-3323). A DFB laser diode with a

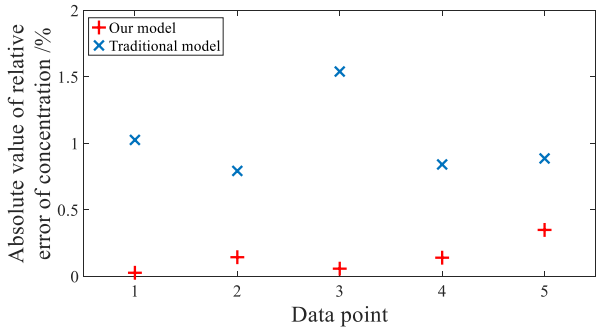


**FIGURE 8.** Scatter plot of the absolute value of relative error of inversed concentration $C$ in simulations.

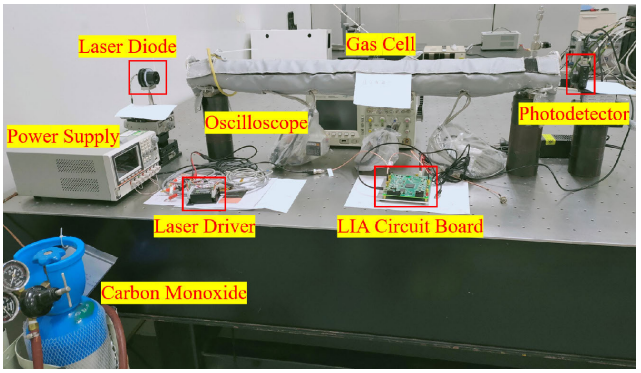


**FIGURE 9.** Photo of the experimental setup.

center wavelength of around 1566 nm and a laser intensity of about 10 mW (Eblana, EP-1566-DM-TP39) is driven by a high stability laser driver (Wavelength, LDTC0520), which integrates two parts of current drive and temperature control. The light emitted from the laser diode firstly passes through a 1-meter directly-passing stainless steel gas cell (Lambert) with calcium fluoride windows, and is detected by the Ge photodetector (Thorlabs, PDA30B2) with a peak response of near 1550 nm. The detector output is connected to the LIA circuit board (Lambert), which integrates the functions of signal generation and lock-in amplification. A digital oscilloscope (Angilent, MSO6104A) is connected to the LIA circuit board output and is used to record the $2f$ signal.

In the experiment, a 5-Hz sawtooth wave scanning signal is used to scan the laser wavelength near the absorption line of CO gas at 1566.64 nm, and a 4000-Hz sinewave modulation signal is used to modulate the laser wavelength. The frequency of the LIA is 8000 Hz. Due to the preamplification of the photodetector and the LIA circuit, the amplitude of the $2f$ signal is different with simulations.

## V. RESULTS AND DISCUSSIONS

### A. PARAMETER FITTING

Using the same method as in simulations, we obtained the parameter fitting dataset as shown in Table 3.

The scatter plots of $\Delta x$ versus $m$ and $k_1(m)$ versus $m$ as shown in Fig. 10 and Fig. 11, which are consistent with the theoretical and simulated scatter plots.

The expressions of the modulation depth and concentration using the fitting dataset are shown in (32) to (34).

**TABLE 3. Parameter Fitting Dataset in Experiments.**

| $C$ | $m$ | $P_{2f\text{-}0}$ | $\Delta x$ |
|---|---|---|---|
| 2.5% | 1.65 | 0.4941 | 3.65 |
| 2.5% | 1.76 | 0.4983 | 3.80 |
| 2.5% | 1.87 | 0.5008 | 4.00 |
| 2.5% | 1.98 | 0.5018 | 4.15 |
| 2.5% | 2.09 | 0.5039 | 4.35 |
| 2.5% | 2.20 | 0.5051 | 4.50 |
| 2.5% | 2.31 | 0.5042 | 4.70 |
| 2.5% | 2.42 | 0.5034 | 4.90 |
| 2.5% | 2.53 | 0.4990 | 5.10 |
| 2.5% | 2.64 | 0.4962 | 5.30 |

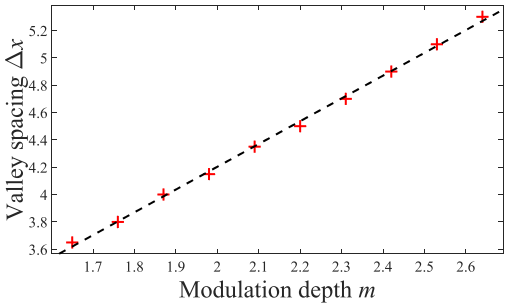


**FIGURE 10. Scatter plot of valley spacing $\Delta x$ versus modulation depth $m$ in experiments.**

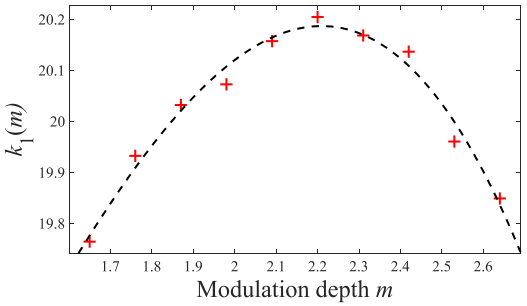


**FIGURE 11. Scatter plot of $k_1(m)$ versus modulation depth $m$ in experiments.**

The coefficient in (32) is similar to that in (29), while the coefficient in (33) to (34) is different from that in (30) to (31) due to the amplification factor of photodetector. The fitted RMSE of modulation depth $m$ is $1.248 \times 10^{-2}$, and $R^2$ is 99.84%. The fitted RMSE of concentration using the improved model is $3.284 \times 10^{-5}$, and that using the traditional model is $1.750 \times 10^{-4}$.

$$m = 0.5991 \times \Delta x - 0.5178 \tag{32}$$

$$C = \frac{P_{2f-0}}{-0.5884 \times m^3 + 2.261 \times m^2 - 1.375 \times m + 18.53} \tag{33}$$

$$C = \frac{P_{2f-0}}{20.03} \tag{34}$$

**TABLE 4. Validation Dataset and Results in Experiments.**

| $C$ | $m$ | $P_{2f\text{-}0}$ | $\Delta x$ | $m_1$ | $C_1$ | $C_2$ |
|---|---|---|---|---|---|---|
| 2.5% | 1.804 | 0.4996 | 3.91 | 1.825 | 2.501% | 2.494% |
| 2.5% | 2.046 | 0.5026 | 4.26 | 2.034 | 2.496% | 2.509% |
| 2.5% | 2.266 | 0.5050 | 4.67 | 2.280 | 2.503% | 2.521% |
| 2.5% | 2.464 | 0.5009 | 4.95 | 2.448 | 2.494% | 2.501% |
| 2.5% | 2.750 | 0.4922 | 5.45 | 2.747 | 2.509% | 2.458% |

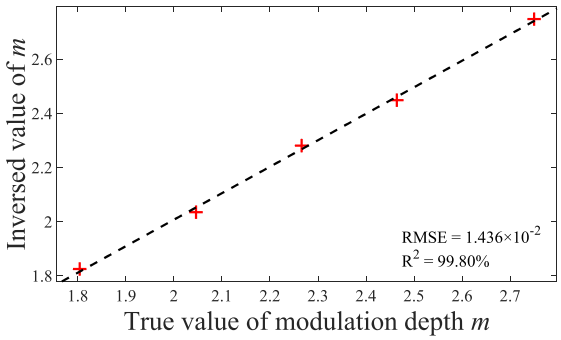


**FIGURE 12. Scatter plot of inversed values versus true values of modulation depth $m$ in experiments.**

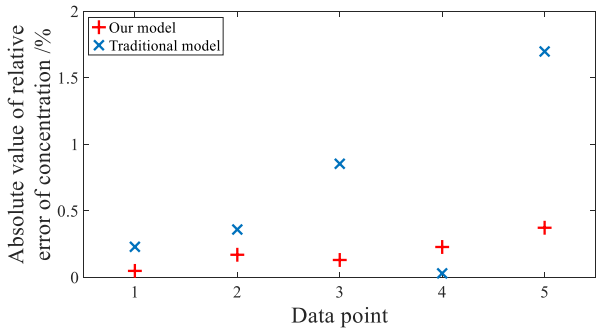


**FIGURE 13. Scatter plot of the absolute value of relative error of inversed concentration $C$ in experiments.**

### B. VALIDATION AND COMPARISON

Using the validation dataset, we obtained the inversion results as shown in Table 4 according to (32) to (34).

The scatter plot of inversed values versus true values of $m$ is shown in Fig. 12, and the RMSE is $1.436 \times 10^{-2}$, $R^2$ is 99.80%, which indicates a high calibration accuracy.

According to Table 4, the RMSE between the inversed values and true values of concentration $C$ using the improved model is $5.468 \times 10^{-5}$ and that using the traditional model is $2.178 \times 10^{-4}$. The scatter plot of the absolute value of relative error of the inversed concentration using both improved and traditional model is shown in Fig. 13.

From Table 4 and Fig. 13, it can be seen that compared with the traditional model (RMSE $= 2.178 \times 10^{-4}$, relative error $<$ 1.70%), the RMSE and relative error of the improved model (RMSE $= 5.468 \times 10^{-5}$, relative error $< 0.37\%$) are reduced by nearly one order of magnitude. The result is consistent with theory and simulations, which verifies the effectiveness of modulation depth calibration using the valley spacing and

the validity and stability of the improved concentration inversion model.

## VI. CONCLUSION

In WMS applications, the changes of modulation depth will cause errors in concentration measurements. In order to eliminate the influence of modulation depth on concentration inversion and improve the measurement accuracy, we first built the modulation depth calibration method using the relationship between the modulation depth and the valley spacing, which does not need the priori information of gas component. Then an improved concentration inversion model was established, where the calibrated modulation depth was added as a parameter. This method is able to improve the concentration inversion accuracy and is immune to the modulation depth variations. The simulation and experimental results verify that the method can accurately calibrate the modulation depth (RMSE in the order of $10^{-2}$) and improve the accuracy of gas concentration measurement by one order of magnitude. This study has a great potential in the applications of the TDLAS and WMS technique especially those with large environmental changes and high accuracy requirements.

The concentration of CO gas used in this study is fixed, and the concentration inversion model only utilizes the second harmonic signal, which relies on the intensity of the laser. Future studies are underway to verify the applicability of the model by using various concentrations, and further improve the measurement accuracy by combining our model with other measurement methods such as the first harmonic normalized second harmonic ($2f/1f$) method.

## REFERENCES

[1] Z. H. Wang, P. F. Fu, and X. Chao, "Laser absorption sensing systems: Challenges, modeling, and design optimization," *Appl. Sci.*, vol. 9, no. 13, pp. 2723-1–2723-27, Jul. 2019, doi: 10.3390/app9132723.

[2] C.-C. Hou, H.-M. Chen, J.-C. Zhang, N. Zhuo, Y.-Q. Huang, R. A. Hogg, D. T. Childs, J.-Q. Ning, Z.-G. Wang, F.-Q. Liu, and Z.-Y. Zhang, "Near-infrared and mid-infrared semiconductor broadband light emitters," *Light, Sci. Appl.*, vol. 7, no. 3, p. 17170, Mar. 2018, doi: 10.1038/lsa.2017.170.

[3] L. Fan, G.-Q. Xia, X. Tang, T. Deng, J.-J. Chen, X.-D. Lin, Y.-N. Li, and Z.-M. Wu, "Tunable ultra-broadband microwave frequency combs generation based on a current modulated semiconductor laser under optical injection," *IEEE Access*, vol. 5, pp. 17764–17771, Aug. 2017, doi: 10.1109/ACCESS.2017.2737665.

[4] Y. Mei, G.-E. Weng, B.-P. Zhang, J.-P. Liu, W. Hofmann, L.-Y. Ying, J.-Y. Zhang, Z.-C. Li, H. Yang, and H.-C. Kuo, "Quantum dot vertical-cavity surface-emitting lasers covering the 'green gap,'" *Light: Sci. Appl.*, vol. 6, no. 1, pp. e16199-1–e16199-7, Jan. 2017, doi: 10.1038/lsa.2016.199.

[5] Z. Khan, N. Ledentsov, L. Chorchos, J.-C. Shih, Y.-H. Chang, N. N. Ledentsov, and J.-W. Shi, "Single-mode 940 nm VCSELs with narrow divergence angles and high-power performances for fiber and free-space optical communications," *IEEE Access*, vol. 8, pp. 72095–72101, Apr. 2020, doi: 10.1109/ACCESS.2020.2987818.

[6] L. Gao, C. Chen, K. Zeng, C. Ge, D. Yang, H. Song, and J. Tang, "Broadband, sensitive and spectrally distinctive SnS2 nanosheet/PbS colloidal quantum dot hybrid photodetector," *Light: Sci. Appl.*, vol. 5, no. 7, pp. e16126-1–e16126-8, Jul. 2016, doi: 10.1038/lsa.2016.126.

[7] R. M. Spearrin, C. S. Goldenstein, I. A. Schultz, J. B. Jeffries, and R. K. Hanson, "Simultaneous sensing of temperature, CO, and $CO_2$ in a scramjet combustor using quantum cascade laser absorption spectroscopy," *Appl. Phys. B, Lasers Opt.*, vol. 117, no. 2, pp. 689–698, Jul. 2014, doi: 10.1007/s00340-014-5884-0.

[8] Z. Zhang, T. Pang, Y. Yang, H. Xia, X. Cui, P. Sun, B. Wu, Y. Wang, M. W. Sigrist, and F. Dong, "Development of a tunable diode laser absorption sensor for online monitoring of industrial gas total emissions based on optical scintillation cross-correlation technique," *Opt. Exp.*, vol. 24, no. 10, pp. 943–955, Apr. 2016, doi: 10.1364/OE.24.00A943.

[9] L. Shao, B. Fang, F. Zheng, X. Qiu, Q. He, J. Wei, C. Li, and W. Zhao, "Simultaneous detection of atmospheric CO and $CH_4$ based on TDLAS using a single 2.3 $\mu$m DFB laser," *Spectrochim. Acta A, Mol. Biomoleular Spectrosc.*, vol. 222, pp. 117118-1–117118-6, Nov. 2019, doi: 10.1016/j.saa.2019.05.023.

[10] M. Lackner, "Tunable diode laser absorption spectroscopy (TDLAS) in the process industries—A review," *Rev. Chem. Eng.*, vol. 23, no. 2, pp. 65–147, Jan. 2007, doi: 10.1515/revce.2007.23.2.65.

[11] C. S. Goldenstein, R. M. Spearrin, J. B. Jeffries, and R. K. Hanson, "Infrared laser-absorption sensing for combustion gases," *Prog. Energy Combustion Sci.*, vol. 60, pp. 132–176, May 2017, doi: 10.1016/j.pecs.2016.12.002.

[12] C. Wang and P. Sahay, "Breath analysis using laser spectroscopic techniques: Breath biomarkers, spectral fingerprints, and detection limits," *Sensors*, vol. 9, no. 10, pp. 8230–8262, Oct. 2009, doi: 10.3390/s91008230.

[13] C. Murzyn, A. Sims, H. Krier, and N. Glumac, "High speed temperature, pressure, and water vapor concentration measurement in explosive fireballs using tunable diode laser absorption spectroscopy," *Opt. Lasers Eng.*, vol. 110, pp. 186–192, Nov. 2018, doi: 10.1016/j.optlaseng.2018.06.005.

[14] P. Kluczynski, J. Gustafsson, A. M. Lindberg, and O. Axner, "Wavelength modulation absorption spectrometry—An extensive scrutiny of the generation of signals," *Spectrochimica Acta B, At. Spectrosc.*, vol. 56, no. 8, pp. 1277–1354, May 2001, doi: 10.1016/s0584-8547(01)00248-8.

[15] R. Arndt, "Analytical line shapes for Lorentzian signals broadened by modulation," *J. Appl. Phys.*, vol. 36, no. 8, pp. 2522–2524, Aug. 1965, doi: 10.1063/1.1714523.

[16] J. Reid and D. Labrie, "Second-harmonic detection with tunable diode lasers—Comparison of experiment and theory," *Appl. Phys. B, Lasers Opt.*, vol. 26, no. 3, pp. 203–210, Nov. 1981, doi: 10.1007/bf00692448.

[17] P. Kluczynski and O. Axner, "Theoretical description based on Fourier analysis of wavelength-modulation spectrometry in terms of analytical and background signals," *Appl. Opt.*, vol. 38, no. 27, pp. 5803–5815, 1999, doi: 10.1364/ao.38.005803.

[18] O. Axner, P. Kluczynski, and Å. M. Lindberg, "A general non-complex analytical expression for the nth Fourier component of a wavelength-modulated Lorentzian lineshape function," *J. Quant. Spectrosc. Radiat. Transf.*, vol. 68, no. 3, pp. 299–317, Feb. 2001, doi: 10.1016/s0022-4073(00)00032-7.

[19] R. Zhang, C. R. Li, Y. Wang, and W. Bai, "Research on modulation frequency and scanning frequency parameters selection of TDLAS system," in *Proc. Int. Conf. EDEP*, Beijing, China, 2016, pp. 1–6.

[20] P. Zhao, J. Tao, C. R. Yu, and Y. Li, "Research on the trace detection of carbon dioxide gas and modulation parameter optimization based on the TDLAS technology," *Proc. SPIE*, vol. 9142, Feb. 2014, Art. no. 914210.

[21] H. Li, G. B. Rieker, X. Liu, J. B. Jeffries, and R. K. Hanson, "Extension of wavelength-modulation spectroscopy to large modulation depth for diode laser absorption measurements in high-pressure gases," *Appl. Opt.*, vol. 45, no. 5, pp. 1052–1061, Feb. 2006, doi: 10.1364/ao.45.001052.

[22] J. Chen, A. Hangauer, R. Strzoda, and M.-C. Amann, "VCSEL-based calibration-free carbon monoxide sensor at 2.3 $\mu$m with in-line reference cell," *Appl. Phys. B, Lasers Opt.*, vol. 102, no. 2, pp. 381–389, Feb. 2011, doi: 10.1007/s00340-010-4011-0.

[23] A. Upadhyay, D. Wilson, M. Lengden, A. L. Chakraborty, G. Stewart, and W. Johnstone, "Calibration-free WMS using a cw-DFB-QCL, a VCSEL, and an edge-emitting DFB laser with *in-situ* real-time laser parameter characterization," *IEEE Photon. J.*, vol. 9, no. 2, pp. 1–17, Apr. 2017, doi: 10.1109/JPHOT.2017.2655141.

[24] H. Chang, S. Feng, X. Qiu, H. Meng, G. Guo, X. He, Q. He, X. Yang, W. Ma, R. Kan, C. Fittschen, and C. Li, "Implementation of the toroidal absorption cell with multi-layer patterns by a single ring surface," *Opt. Lett.*, vol. 45, no. 21, pp. 5897–5900, Nov. 2020, doi: 10.1364/OL.404198.

[25] X. Guo, F. Zheng, C. Li, X. Yang, N. Li, S. Liu, J. Wei, X. Qiu, and Q. He, "A portable sensor for *in-situ* measurement of ammonia based on near-infrared laser absorption spectroscopy," *Opt. Lasers Eng.*, vol. 115, pp. 243–248, Apr. 2019, doi: 10.1016/j.optlaseng.2018.12.005.

[26] J. Chen, A. Hangauer, R. Strzoda, and M.-C. Amann, "Accurate extraction method for the FM response of tunable diode lasers based on wavelength modulation spectroscopy," *Appl. Phys. B, Lasers Opt.*, vol. 90, no. 2, pp. 243–247, Feb. 2008, doi: 10.1007/s00340-007-2848-7.
[27] J. Deng, W.-L. Chen, W.-F. Wang, Y. He, and B.-L. Zhang, "Study on online detection method of methane gas in coal mine based on TDLAS technology," in *Proc. 11th IMVC*, Xi'an, China, Aug. 2018, pp. 318–332.
[28] C. Yang, L. Mei, H. Deng, Z. Xu, B. Chen, and R. Kan, "Wavelength modulation spectroscopy by employing the first harmonic phase angle method," *Opt. Exp.*, vol. 27, no. 9, pp. 12137–12146, Apr. 2019, doi: 10.1364/OE.27.012137.
[29] A. Upadhyay and A. L. Chakraborty, "Calibration-free 2f WMS with *in situ* real-time laser characterization and 2f RAM nulling," *Opt. Lett.*, vol. 40, no. 17, pp. 4086–4089, Sep. 2015, doi: 10.1364/ol.40.004086.
[30] C. Zhu, J. Chang, P. Wang, W. Wei, Q. Wang, F. Wang, and S. Zhang, "Continuously wavelength-tunable light source with constant-power output for elimination of residual amplitude modulation," *IEEE Sensors J.*, vol. 15, no. 1, pp. 316–321, Jan. 2015, doi: 10.1109/JSEN.2014.2343653.
[31] J. Sun, J. Chang, F. Wang, Q. Zhang, Z. Wang, Y. Xie, Z. Zhang, and Y. Feng, "Tuning efficiency of distributed feedback laser diode for wavelength modulation spectroscopy," *IEEE Sensors J.*, vol. 19, no. 21, pp. 9722–9727, Nov. 2019, doi: 10.1109/JSEN.2019.2927043.
[32] I. E. Gordon *et al.*, "The HITRAN2016 molecular spectroscopic database," *J. Quant. Spectrosc. Radiat. Transf.*, vol. 203, pp. 3–69, Dec. 2017, doi: 10.1016/j.jqsrt.2017.06.038.

**YUN PAN** was born in Nantong, Jiangsu, China, in 1992. She received the B.S. degree in geochemistry from the University of Science and Technology of China, Anhui, China, in 2015. She is currently pursuing the Ph.D. degree in optical engineering with the Changchun Institute of Optics, Fine Mechanics and Physics, Chinese Academy of Sciences, Changchun, China. Her current research interests include the applications of tunable diode laser absorption spectroscopy technology and gas detection in industrial process control.

**YI LI** was born in Xilingol League, Inner Mongolia, China, in 1992. He received the B.E. degree in mechanical engineering and automation from Zhejiang University, China, in 2014, and the Ph.D. degree in optical engineering from the Changchun Institute of Optics, Fine Mechanics and Physics, Chinese Academy of Sciences, Changchun, China, in 2020. Since 2020, he has been with the Changchun Institute of Optics, Fine Mechanics and Physics, Chinese Academy of Sciences. His research interests include the opto-mechatronics technology for space optical remote sensing instruments and design and optimization of opto-mechanical structure.

**CHANGXIANG YAN** was born in Honghu, Hubei, China, in 1973. He received the M.S. degree in engineering from Zhejiang University, Zhejiang, China, in 1998, and the Ph.D. degree from the Changchun Institute of Optics, Fine Mechanics and Physics, Chinese Academy of Sciences, Changchun, China, in 2001.

Since 2010, he has been with the Director of the Space Optics Laboratory, Changchun Institute of Optics, Fine Mechanics and Physics, Chinese Academy of Sciences. His research interests include opto-mechatronics technology for space optical remote sensing instruments, multispectral and hyper-spectral spatial remote sensing imaging, polarization detection, and space surveillance.

**JING YUAN** was born in Changchun, Jilin, China, in 1993. She received the B.S. degree in optical information science and technology from Jilin University, China, in 2016. She is currently pursuing the Ph.D. degree in optical engineering with the Changchun Institute of Optics, Fine Mechanics and Physics, Chinese Academy of Sciences, Changchun, China. Her current research interests include the application of spectra, hyper-spectral remote sensing, and the application of remote sensing in soil.

**YIJIE REN** was born in Changzhi, Shanxi, China, in 1994. He received the B.S. degree in measurement and control technology and instrument from the Changchun University of Science and Technology, China, in 2018. He is currently pursuing the Ph.D. degree in optical engineering with the Changchun Institute of Optics, Fine Mechanics and Physics, Chinese Academy of Sciences, Changchun, China. His current research interests include cavity ring-down spectroscopy and trace gas detection.